Packing of stiff rods on ellipsoids: Geometry

Doron Grossman,* Eytan Katzav,† and Eran Sharon‡
Racah Institute of Physics, Hebrew University, Jerusalem 9190401, Israel

(Received 12 October 2020; accepted 17 December 2020; published 7 January 2021)

We suggest a geometrical mechanism for the ordering of slender filaments inside nonisotropic containers, using cortical microtubules in plant cells and the packing of viral genetic material inside capsids as concrete examples. We show analytically how the shape of the cell affects the ordering of phantom elastic rods that are not self-avoiding (i.e., self-crossing is allowed). We find that for oblate cells, the preferred orientation is along the equator, while for prolate spheroids with an aspect ratio close to 1, the orientation is along the principal (long axis). Surprisingly, at a high enough aspect ratio, a configurational phase transition occurs and the rods no longer point along the principal axis, but at an angle to it, due to high curvature at the poles. We discuss some of the possible effects of self-avoidance using energy considerations. These results are relevant to other packing problems as well, such as the spooling of filament in the industry or spider silk inside water droplets.

DOI: 10.1103/PhysRevE.103.013001

I. INTRODUCTION

The packing of filaments inside volumes of a given shape is an important problem in many fields, from the packing of genetic material inside viral capsids [1–5] through ordering microtubules near plant cell walls [6–8] to the spooling of filaments in industrial applications [9–11] and other biopolymers such as spider silk [12–15]. These types of problems are difficult as they typically involve a compromise between elastic energy and entropic constraints. As a result, most approaches to these problems involve highly symmetric volumes and are mostly numerical. This paper's aim is to gain further analytical understanding of systems that are not highly symmetric, using differential geometry. A study of entropic effects and self-avoidance is largely postponed to a later paper. As concrete examples, we consider plant cells where shape regulation is important and microtubules play a significant role, and the packing of genetic material inside viral capsids. While these two examples seem very different, both are essentially problems of packing long semiflexible filaments. Additionally, the authors hope that this work will serve as an inspiration for applying similar methods from differential geometry to study other systems, involving geometric constraints on elastic bodies, and not only the packing of filaments on surfaces.

In the context of plant tissue, the confinement of microtubules (MT) in the cell membrane, and especially the possible transition from disordered to partially ordered packing, is thought to be the origin of important morphogenetic and growth regulating mechanisms. The location of leaves on the stem, anisotropic cell expansion, as in roots and stems, and the evolution of anisotropic mechanical properties of extended leaf tissue are a few examples in which mechanical and geometrical asymmetries appear. In plant cells, cellulose fibrils in the cell wall are the carrier of mechanical load. The orientation of cortical MT dictates the orientation of cellulose fibrils deposition in the cell wall [7]. Therefore, anisotropic MT orientation would lead to anisotropic cellulose deposition, and thus to anisotropic mechanical properties of the cell. This, in turn, would lead to its anisotropic growth and to shape evolution of the tissue. But what sets MT orientation at the single cell level? The suggestion that mechanical stress directly affects MT orientation was supported by pointing to the correlations between MT orientation and the directions of principal stresses in evolving meristems [6]. On the other hand, it is not clear how stress or strain in the cell wall can affect the cell membrane [16,17]. In addition, the effect of applied stress on the mechanical properties of a leaf appeared only after a delay of several hours [18]. This suggests that an integral mechanism, which is common in other growth regulation mechanisms [19,20], could be in action. Alternative approaches suggest that the cell shape, and particularly its anisotropy, is a dominant factor in MT ordering. The two approaches are, in fact, closely related: Considering a circular cell, an integral over the strain determines the cell's anisotropy. We therefore pose the questions of what are the leading effects of cell shape on the disordered-aligned transition of MT.

In the context of viral capsids, there is an ultimate necessity for the genetic material to be orderly packed inside the capsid in order to assure effective infection. This is so important because once the genetic material is packed inside the capsid, it has no active sources of energy to support its injection, except for the elastic energy stored in the structure. It has been convincingly argued [1,2,4] that the size of the capsid plays an important role in piloting toward an ordered structure based on both entropic and energetic considerations, showing that active biological control over ordering the spool could be seriously reduced. In particular, a continuous phase transition

*doron.grossman@mail.huji.ac.il
†eytan.katzav@mail.huji.ac.il
‡erans@mail.huji.ac.il

between a disordered phase (for large capsids) and an ordered phase (for small capsids) has been found. The spontaneous formation of virus capsids from multiple copies of capsid proteins is itself a fascinating example of supramolecular self-assembling processes [21]. Most known viruses protect their genome with icosahedral capsids, which is often modeled as a spherical cavity. However, other capsid morphologies exist as well, notably elongated, often ellipsoid, structures. The bacteriophage $\phi 29$ has elongated capsids with a size of about 42 nm $\times$ 54 nm leading to an aspect ratio of 4 : 5 [22,23]. The capsid of archaeal virus Sulfolobus ellipsoid virus 1 (SEV1) [24] is that of a prolate ellipsoid with principal axes of 78 nm $\times$ 115 nm, hence an aspect ratio of about 2 : 3. Other important examples include the human virus HIV-1, where experiments have demonstrated the self-assembly of viral capsid proteins into elongated shapes both *in vitro* and *in vivo* [25] with varying aspect ratios depending on the precise conditions during the assembly process, notably the interaction between the building block proteins. An interesting example is the case of extremely elongated capsids in mutant T4 phages [26] with aspect ratios in the range 1 : 2–1 : 3 leading to a twisted toroidal configuration of DNA inside them. An immediate question that comes to mind is as follows: does the shape of the capsid affect the ordering phase transition of the genetic material in the capsid compared to the spherical case? Simulations performed by different groups [1,9,22,27] indicate that packings in oblate spheroids and scalene ellipsoids are energetically preferred over spheres. In simple terms, it seems that the elongated container tends to order the structure more than a spherical one. Furthermore, it was observed in simulations [22,23,28–30] that the kind of order of the genetic material changes, and attains a nematically ordered structure with twist (also called twisted toroidal conformations [28]), as opposed to a spool-like one in spherical capsids. The different simulations are not clear about the source of this effect. Some suggest that the toroidal packing arranges itself along the longest possible dimension to minimize the bending stress (and hence the elastic energy) [28], while others put more of an emphasis on the entropic effect [31]. In this paper, we want to clarify the energetic aspects of packing an elastic rod, and in particular the enhanced ordering emanating from the elongated geometry, while in a future publication we will focus on entropic effects.

II. PACKING OF PHANTOM FILAMENTS ON THE SURFACE OF AN ELLIPSOID

We begin by assuming a phantom, i.e., not a self-avoiding, unstretchable, filament of thickness t whose midline is given by $\mathbf{R}(s) = \{X(s), Y(s), Z(s)\}$, where s is the arc length along the rod [i.e., $|\partial_s \mathbf{R}(s)| = 1$, or a unit speed curve]. The bending energy of such a rod is

$$E = \frac{\varepsilon t^4}{2} \int |\ddot{\mathbf{R}}(s)|^2 \, ds = \frac{\varepsilon t^4}{2} \int (\ddot{X}^2 + \ddot{Y}^2 + \ddot{Z}^2) \, ds, \quad (1)$$

where $\ddot{Q} = \partial_s^2 Q$ is the second derivative of the quantity $Q(s)$, and ε is the rod's Young's modulus. At zero temperature, the rod's configuration is the global minimizer of Eq. (1) subjected to the constraint of lying on the surface of an ellipsoid, $X^2(s) + Y^2(s) + Z^2(s)/(1+\delta)^2 = 1$, where $\delta > -1$ is called the flattening of the ellipsoid, and it is related to the usual definition of eccentricity, e, via $e^2 = \delta(2+\delta)$ [32–34]. A vanishing flattening, $\delta = 0$, corresponds to a sphere. Negative values of δ in the range $-1 < \delta < 0$ describe an oblate spheroid, while positive values, $\delta > 0$, describe a prolate spheroid. The problem of finding the global energy minimizer is difficult, as the system is clearly highly frustrated. We therefore use a geometrical approach, and we describe the rod using its curvatures rather than the configuration $\mathbf{R}$. We start by assigning a generalized Frenet-Serret frame (an orthonormal frame transported along a curve; see [35–37]), $\{\mathbf{t}_1, \mathbf{t}_2, \mathbf{t}_3\}$ being the tangent, binormal, and normal vectors of the rod, respectively, as follows. Given $\mathbf{f} = \{X(x,y), Y(x,y), Z(x,y)\}$, the surface configuration (x, y being coordinates *on the surface*), and $\hat{\mathbf{n}}$ the normal to the surface, we choose a local orthonormal in-plane frame along the rod, using a Darboux frame on the surface $\{\partial_x \mathbf{f}, \partial_y \mathbf{f}, \hat{\mathbf{n}}\}$ (note that $\partial_x \mathbf{f}, \partial_y \mathbf{f}$ are not orthonormal). We define the Frenet-Serret frame, $\{\mathbf{t}_1, \mathbf{t}_2, \mathbf{t}_3\}$, and the in-plane surface tangent and normal vectors e_1^μ and e_2^μ:

$$\mathbf{t}_1 = \dot{\mathbf{R}} = e_1^\mu \partial_\mu \mathbf{f}, \quad (2a)$$

$$\mathbf{t}_2 = e_2^\mu \partial_\mu \mathbf{f}, \quad (2b)$$

$$\mathbf{t}_3 = \hat{\mathbf{n}}. \quad (2c)$$

Orthonormality dictates that the inner products satisfy $e_1^\mu e_{1\mu} = a_{\mu\nu} e_1^\mu e_1^\nu = 1 = e_2^\mu e_{2\mu}$ and $e_1^\mu e_{2\mu} = 0$, where $a_{\mu\nu} = \partial_\mu \mathbf{f} \cdot \partial_\nu \mathbf{f}$ is the induced metric on the surface, and $\mu, \nu \in \{x, y\}$.

It is then straightforward to show that $\mathbf{t}_\alpha$, $\alpha \in \{1, 2\}$, satisfy the equations

$$\begin{aligned} \dot{\mathbf{t}}_\alpha &= \partial_s \mathbf{t}_\alpha \\ &= \left(\partial_s e_\alpha^\mu\right) \partial_\mu \mathbf{f} + e_1^\mu e_\alpha^\nu \partial_\mu \partial_\nu \mathbf{f} \\ &= e_1^\mu e_\alpha^\nu b_{\mu\nu} \mathbf{t}_3 - \kappa_g \sum_\beta \epsilon_{\alpha\beta} e_\beta^\mu \partial_\mu \mathbf{f}, \end{aligned} \quad (3)$$

and $\mathbf{t}_3$ satisfies

$$\dot{\mathbf{t}}_3 = -\sum_\alpha e_1^\mu e_\alpha^\nu b_{\mu\nu} \mathbf{t}_\alpha. \quad (4)$$

Here $b_{\mu\nu} = \partial_\mu \partial_\nu \mathbf{f} \cdot \hat{\mathbf{n}}$ is the second fundamental form of the confining surface, κ_g is the geodesic curvature of the rod on the surface, and $\epsilon_{\alpha\beta}$ is the 2×2 antisymmetric (Levi-Civita) symbol. Deriving Eq. (3), we used the fact that for a general curve, namely a nongeodesic one, on the surface e_1^μ and e_2^μ are transported via the equation

$$\nabla_s e_\alpha^\mu = \partial_s e_\alpha^\mu + e_1^\rho e_\alpha^\sigma \Gamma_{\rho\sigma}^\mu = -\kappa_g \sum_\beta \epsilon_{\alpha\beta} \, e_\beta^\mu, \quad (5)$$

where ∇_s is the covariant derivative along the curve, and the Christoffel symbols are given in a configuration

$$a_{\rho\lambda} \Gamma_{\mu\nu}^\lambda = \partial_\mu \partial_\nu \mathbf{f} \cdot \partial_\rho \mathbf{f}. \quad (6)$$

Equations (3) and (4) can be rewritten in matrix form as

$$\begin{pmatrix} \dot{\mathbf{t}}_1(s) \\ \dot{\mathbf{t}}_2(s) \\ \dot{\mathbf{t}}_3(s) \end{pmatrix} = -\begin{pmatrix} 0 & \kappa_g & -l \\ -\kappa_g & 0 & m \\ l & -m & 0 \end{pmatrix} \begin{pmatrix} \mathbf{t}_1(s) \\ \mathbf{t}_2(s) \\ \mathbf{t}_3(s) \end{pmatrix}, \quad (7)$$

where we defined the curvatures

$$l = e_1^\mu e_1^\nu b_{\mu\nu}, \tag{8a}$$

$$m = -e_1^\mu e_2^\nu b_{\mu\nu}. \tag{8b}$$

The formal solution of Eq. (7) is

$$\begin{pmatrix}\mathbf{t}_1(s)\\ \mathbf{t}_2(s)\\ \mathbf{t}_3(s)\end{pmatrix} = T_s\left\{\exp\left[-\int_0^s ds'\begin{pmatrix}0 & \kappa_g & -l\\ -\kappa_g & 0 & m\\ l & -m & 0\end{pmatrix}\right]\right\}\begin{pmatrix}\mathbf{t}_1(0)\\ \mathbf{t}_2(0)\\ \mathbf{t}_3(0)\end{pmatrix}, \tag{9}$$

where we use the definition of the position ordering operator T_s,

$$T_s \exp\left[\int_0^s M ds'\right] = \lim_{k\to\infty} e^{M(s_k)\Delta s} e^{M(s_{k-1})\Delta s}\cdots e^{M(s_1)\Delta s} e^{M(s_0)\Delta s}, \tag{10}$$

where $\Delta s = \frac{s}{k}$ and $s_k = k\Delta s$. The rod configuration is then given by

$$\mathbf{R}(s) = \mathbf{R}(0) + \int_0^s \mathbf{t}_1(s')\, ds'. \tag{11}$$

The elastic energy (1) assumes the form

$$E = \frac{\varepsilon t^4}{2}\int ds\left(\kappa_g^2 + l^2\right). \tag{12}$$

While this seems to be a simpler functional than the one given in Eq. (1), one must remember that l itself is a functional of the geodesic curvature, $\kappa_g(s)$ [via Eq. (5)]. Since we are searching for global minimizers (for infinitely long rods), we seek to minimize the total energy per unit length,

$$\bar{E} = \frac{E}{L} = E_0\frac{\int\left(\kappa_g^2 + l^2\right) ds}{\int ds}, \tag{13}$$

where we define the energy scale $E_0 = \frac{\varepsilon t^4}{2}$.

Equation (13) reveals an important property of the energy minimizing problem: while the normal curvature, l, is a property of the surface, the geodesic curvature, k_g, can be eliminated by a proper selection of the rod configuration. These configurations are geodesics, which locally minimize Eq. (13). As shown later (Appendix A), for any positive flattening, $\delta > 0$, no geodesic is a global minimizer. However, the true global minimizer cannot deviate significantly from a geodesic (see Appendix B). Therefore, we conclude that geodesics are good approximations, and we limit ourselves to their study, which significantly simplifies the problem.

We begin by parametrizing the surface of the ellipsoid using θ (polar) and ϕ (azimuthal) angles, and subsequently finding the geodesics in terms of these coordinates:

$$\begin{aligned} X &= \cos\phi\sin\theta,\\ Y &= \sin\phi\sin\theta,\\ Z &= (1+\delta)\cos\theta. \end{aligned} \tag{14}$$

The metric **a**, the second fundamental form **b**, and the shape operator (extrinsic curvature) **S** [38] of the surface are then given by

$$\mathbf{a} = \begin{pmatrix}1+\delta(2+\delta)\sin^2\theta & 0\\ 0 & \sin^2\theta\end{pmatrix}, \tag{15}$$

$$\mathbf{b} = -\frac{1+\delta}{\sqrt{1+\delta(2+\delta)\sin^2\theta}}\begin{pmatrix}1 & 0\\ 0 & \sin^2\theta\end{pmatrix}, \tag{16}$$

$$\mathbf{S} = \mathbf{a}^{-1}\mathbf{b} = -\begin{pmatrix}\frac{1+\delta}{[1+\delta(2+\delta)\sin^2\theta]^{3/2}} & 0\\ 0 & \frac{1+\delta}{\sqrt{1+\delta(2+\delta)\sin^2\theta}}\end{pmatrix}. \tag{17}$$

Since the metric is independent of ϕ, there is a conserved, conjugate "angular momentum" ω, which is related to the "angular velocity" $\dot{\phi}$, and is the generator of rotations around the symmetry axis of the ellipsoid found by solving the geodesic equation for the ϕ coordinate [38]:

$$\frac{d}{ds}\left(a_{\phi\mu}\frac{dx^\mu}{ds}\right) = 0. \tag{18}$$

Since the metric is diagonal, only $a_{\phi\phi} = \sin^2\theta$ contributes to the sum,

$$\frac{d}{ds}\left(a_{\phi\phi}\frac{d\phi}{ds}\right) = 0. \tag{19}$$

In other words, this is a constant, which we mark by ω,

$$\sin^2\theta\frac{d\phi}{ds} = \omega = \text{const}. \tag{20}$$

Thus

$$\dot{\phi}(s) = \frac{\omega}{\sin^2\theta}, \tag{21}$$

where arc-length normalization of s requires $-1 \leqslant \omega \leqslant 1$. Physically, one can interpret $\omega = \cos\psi$, where ψ is the angle between the geodesic and the equator. Thus a geodesic along the equator has $\omega = \pm 1$, while a geodesic passing through the poles has $\omega = 0$ [see Figs. 2 and 5(c) for examples].

Instead of solving the geodesic equation for θ, we may impose normalization, $e_1^\mu e_1^\nu a_{\mu\nu} = 1$, and get the equation

$$(1 + 2\delta\sin^2\theta + \delta^2\sin^2\theta)\dot{\theta}^2 = 1 - \frac{\omega^2}{\sin^2\theta}. \tag{22}$$

By taking $\sin^2\theta$ as a common factor, we get

$$\left(\frac{1}{\sin^2\theta} + 2\delta + \delta^2\right)\sin^2\theta\dot{\theta}^2 = 1 - \frac{\omega^2}{\sin^2\theta} \tag{23}$$

leading to

$$\left(\frac{d}{ds}\cos\theta\right)^2 = \frac{1 - \frac{\omega^2}{\sin^2\theta}}{\left(\frac{1}{\sin^2\theta} + 2\delta + \delta^2\right)}. \tag{24}$$

Rewriting everything in terms of $\cos\theta$, we get the equation

$$\left(\frac{d}{ds}\cos\theta\right)^2 = \frac{1-\omega^2-\cos^2\theta}{[(1+\delta)^2-2\delta\cos^2\theta-\delta^2\cos^2\theta]}, \tag{25}$$

which, after defining $x(s)=\cos[\theta(s)]$ and marking $\dot{x}=\frac{dx}{ds}$, turns into

$$(\dot{x})^2 = \frac{1-\omega^2-x^2}{(1+\delta)^2-(2\delta+\delta^2)x^2}. \tag{26}$$

Separating variables and integrating, we obtain

$$\int \frac{\sqrt{(1+\delta)^2-(2\delta+\delta^2)x^2}\,dx}{\sqrt{1-\omega^2-x^2}} = \pm\int ds + s_0. \tag{27}$$

This equation is integrable, giving rise to

$$(1+\delta)\mathcal{E}\left[\sin^{-1}\left(\frac{x}{\sqrt{1-\omega^2}}\right)\middle|\frac{\delta(\delta+2)(1-\omega^2)}{(\delta+1)^2}\right] = \pm s + s_0, \tag{28}$$

where $\mathcal{E}[\theta|m]=\int_0^\theta\sqrt{1-m\sin^2\phi}\,d\phi$ is the incomplete elliptic integral of the second kind [39], and s_0 is determined by initial conditions. To find geodesics, we now need to integrate Eq. (21), which can be done numerically. However, by virtue of rotational symmetry about the polar axis of the ellipsoid ($a_{\mu\nu}$ is independent of ϕ, and geodesics are parametrized by ω alone), we can disregard exact solutions of $\phi(s)$ when looking for minimizing geodesics, and we can immediately look for a minimizer of Eq. (13) [see Eq. (30)].

Evaluation of $\bar{E}$ on geodesics is achieved by using $\kappa_g=0$ and $e_1^\mu=(\dot{\theta},\dot{\phi})$, which is given by Eqs. (22) and (21). Additionally, by virtue Eq. (28), instead of integrating over s we may integrate over θ (or rather over x) using

$$\frac{ds}{dx} = \sqrt{\frac{(1+\delta)^2-\delta(2+\delta)x^2}{1-\omega^2-x^2}}. \tag{29}$$

Thus, focusing on geodesics, we look to minimize the following energy functional:

$$\frac{\bar{E}(\omega,\delta)}{E_0} = \frac{\int E\,ds}{\int ds} = \frac{\int_{-\sqrt{1-\omega^2}}^{\sqrt{1-\omega^2}} \frac{(1+\delta)^2[1+\delta(2+\delta)\omega^2]^2}{[1+\delta(\delta+2)(1-x^2)]^3}\sqrt{\frac{1+(1-x^2)\delta(2+\delta)}{1-x^2-\omega^2}}\,dx}{\int_{-\sqrt{1-\omega^2}}^{\sqrt{1-\omega^2}}\sqrt{\frac{1+(1-x^2)\delta(2+\delta)}{1-x^2-\omega^2}}\,dx} \tag{30}$$

$$= \frac{2[2+\delta(2+\delta)(1+\omega^2)]\mathcal{E}\left[\frac{\delta(2+\delta)(1-\omega^2)}{(1+\delta)^2}\right]-2[1+\delta(2+\delta)\omega^2]\mathcal{K}\left[\frac{\delta(2+\delta)(1-\omega^2)}{(1+\delta)^2}\right]}{3(1+\delta)^2\mathcal{E}\left[\frac{\delta(2+\delta)(1-\omega^2)}{(1+\delta)^2}\right]} \tag{31}$$

$$= \frac{2[2+\delta(2+\delta)(1+\omega^2)]}{6(1+\delta)^2} - \frac{2[1+\delta(2+\delta)\omega^2]\mathcal{K}\left[\frac{\delta(2+\delta)(1-\omega^2)}{(1+\delta)^2}\right]}{3(1+\delta)^2\mathcal{E}\left[\frac{\delta(2+\delta)(1-\omega^2)}{(1+\delta)^2}\right]}, \tag{32}$$

where $\mathcal{E}[m]=\int_0^{\pi/2}\sqrt{1-m\sin^2\theta}\,d\theta$ and $\mathcal{K}[m]=\int_0^{\pi/2}(\sqrt{1-m\sin^2\theta})^{-1}\,d\theta$ are the complete elliptic integrals of the second and first kind [39], respectively. Plotting $\bar{E}$ for different values of δ as a function of ω (see Fig. 1), it is easily seen that for $\delta<0$ only $\omega=\pm1$ are the minima. This is true for every $-1<\delta<0$, and, as seen in Appendix A, these solutions are stable. We therefore conclude that equatorial geodesics are the global minimizers for oblate spheroids [see Fig. 2(a)]. Not surprisingly, in the case of a sphere ($\delta=0$) we find that any geodesic is a global minimizer. These results (for $\delta\leqslant 0$) are indeed very intuitive. In contrast, a more complex behavior arises in the case of prolate spheroids ($\delta>0$), where we observe a sharp transition at a critical flattening δ^* [Fig. 1; see Figs. 2(b) and 2(c) for visualization of possible curves].

We mark by $\omega_m(\delta)$ the minimizer of $\bar{E}(\omega,\delta)$, and its energy is denoted by $\bar{E}(\omega_m(\delta))=\bar{E}(\omega_m(\delta),\delta)$, i.e., the globally minimizing geodesic, as a function of the flattening, δ, and we plot it in Fig. 3. We find that for $0<\delta\leqslant\delta^*$, polar geodesics ($\omega_m=0$) are the minimizers of $\bar{E}$, while for $\delta>\delta^*$, $\omega_m(\delta)\neq 0$. Solving numerically the requirement that the extremum at $\omega=0$ becomes a saddle $\frac{\partial^2\bar{E}}{\partial\omega^2}|_{\omega=0}=0$, where

$$\left.\frac{\partial^2\bar{E}}{\partial\omega^2}\right|_{\omega=0} = \frac{E_0}{3}\left[5-\frac{4}{(1+\delta)^2}+\frac{\mathcal{K}\left[\frac{\delta(2+\delta)}{(1+\delta)^2}\right]}{\mathcal{E}\left[\frac{\delta(2+\delta)}{(1+\delta)^2}\right]}\left(\frac{1}{(1+\delta)^2}\frac{\mathcal{K}\left[\frac{\delta(2+\delta)}{(1+\delta)^2}\right]}{\mathcal{E}\left[\frac{\delta(2+\delta)}{(1+\delta)^2}\right]}-2\right)\right], \tag{33}$$

we find that $\delta^*\simeq 2.917$. It can now be shown that near the transition, as $\delta\to\delta^{*+}$, $\omega_m(\delta)\sim\sqrt{\delta-\delta^*}$.

In the limit of an infinitely eccentric ellipsoid, we get

$$\frac{\bar{E}}{E_0}\xrightarrow[\delta\to\infty]{}\frac{2}{3}+\frac{\omega^2}{3}\left(2-\frac{\mathcal{K}[1-\omega^2]}{\mathcal{E}[1-\omega^2]}\right), \tag{34}$$

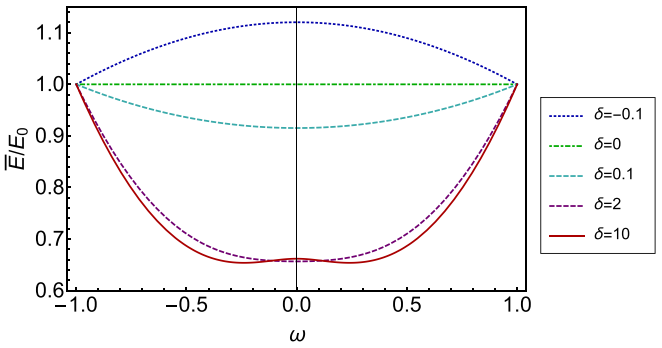

FIG. 1. Mean energy per unit length, $\bar{E}$, of geodesics (parametrized by the angular momentum ω) for different values of δ as indicated in the figure. All oblate spheroids ($\delta < 0$) are qualitatively the same—polar geodesics ($\omega = 0$) have the maximal energy, while equatorial ones $\omega = \pm 1$ are minimal. In the case of prolate spheroids $\delta > 0$, the situation is very different: for $0 < \delta < \delta^*$, $\omega_m = 0$ is the minimal geodesic, while for $\delta^* < \delta$, two symmetric solutions arise $\pm\omega_m(\delta)$, which tend to the asymptotic value $\omega_m(\infty) = 0.255$ for extremely eccentric ellipsoids.

whose minimizer is $\omega \simeq \pm 0.255\ldots$. This value corresponds to geodesics that intersect the equator at an angle of $\psi \simeq 75.22^\circ$ relative to the equator.

Why does this transition happen? Simply put, it is because for large δ's, the curvature at the poles becomes very large and dominant. Thus, the minimizing geodesic is such that it does not pass through the poles on one hand, yet it is still mainly directed toward the poles, so as to gain as much as possible from the large difference in principal curvature values. This result raises the question of whether there is a nongeodesic solution that has a lower mean energy even for small δ, one that does not pass through the poles. Indeed, as seen in Appendix B, there must be such a solution, yet this solution is still close to a geodesic, and in any case the solution to the real physical problem must also take into account temperature, activity, and self-avoidance. Our analysis sheds light on some aspects of the mechanisms governing the actual shape and suggests that a proper treatment should take into account the surface's shape effect on the final configuration, as it serves as an "external field" biasing the rod to align along the symmetries of the problem.

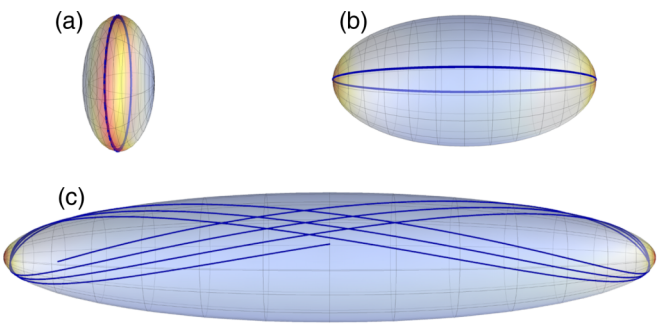

FIG. 2. Visualization of ellipsoids and their minimizing geodesics, for three different flattening (δ) values. Surface color represents Gaussian curvature: high curvature, red; low curvature, light blue. (a) $\delta = -0.5$, an equatorial geodesic ($\omega = 1$) is the global minimizer; (b) $\delta = 1 < \delta^*$, a polar geodesic ($\omega = 0$ is the global minimizer); and (c) $\delta = 4 > \delta^*$, in which the global minimizer ($0 < \omega < 0.255$) does not pass through the poles (only a finite portion is shown).

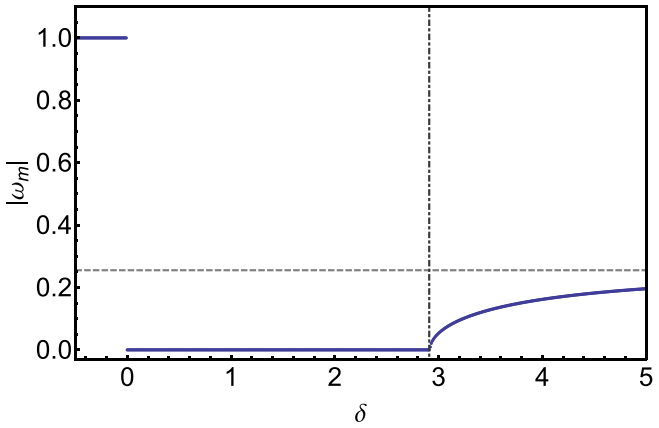

FIG. 3. $|\omega_m(\delta)|$ as a function of δ. Note that $|\omega_m(\delta < 0)| = 1$. The gray dashed horizontal line is the asymptote $|\omega_m(\infty)| = 0.255$; the vertical dot-dashed line marks the critical value $\delta^* = 2.917\,56$.

Finally, for $\delta \neq 0$, these solutions given above, which all have a preferred direction (i.e. they are not isotropic), are clearly preferable to any other curve that covers the ellipsoid isotropically. Any isotropic solution that covers the ellipsoid must have geodesic curvature, but for infinitely long filaments one may create such a curve by slowly changing ω along a curve. In this "quasistatic" limit, we change ω without introducing any geodesic curvature. Such a curve gives a lower bound on the energy of isotropic curves and is given by averaging $\bar{E}$ over all ω,

$$\bar{E}_{\rm iso}(\delta) = \frac{\int \bar{E}(\omega, \delta)\, d\omega}{\int \bar{E}(\omega)\, d\omega}. \tag{35}$$

From Fig. 4 it is clearly seen that a directional (nonisotropic) configuration is preferable compared to an isotropic configuration, since the dashed blue line corresponding to $\bar{E}_{\rm iso}(\delta)$ is higher than the red solid line describing the energy of the globally minimizing geodesics $\bar{E}(\omega_m(\delta))$.

III. THE ROLE OF SELF-AVOIDANCE

Before we conclude, a few words are in order on the possible effect of self-avoidance. Naturally, a full mechanical treatment of self-avoiding filaments is difficult. However, we may still have a few insights using our geometrical approach. We have shown that as the ellipsoid elongates, and due to the growing curvature at the poles, a transition occurs so that the minimizing configuration is no longer a polar geodesic. In the presence of self-avoidance, this transition is likely to occur later, at higher values of δ, depending on the strength of the self-avoiding interaction. The reason is that a polar geodesic-like path [see Fig. 5(a)] allows (especially for thin filaments) a nonintersecting packing, in contrast to the solution for $\delta > \delta^*$. The energy associated with a self-avoiding (SA) packing is

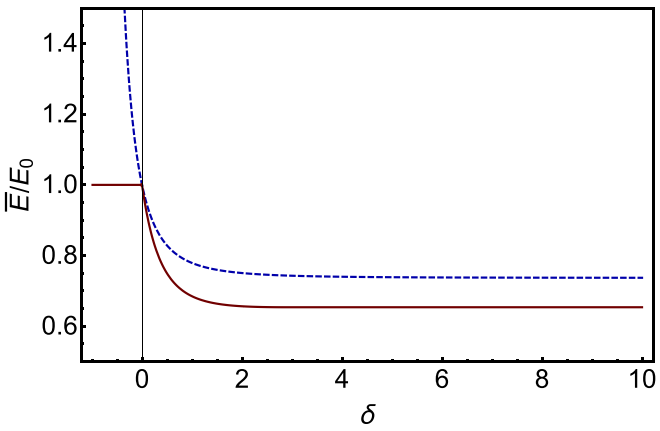

FIG. 4. Comparison of the energy $\bar{E}_{\rm iso}(\delta)$ of a slowly varying isotropically oriented curve (blue dashed line) vs the minimizing geodesic's energy $\bar{E}(\omega_m(\delta))$ as a function of δ (solid red line).

(see Appendix C)

$$\begin{aligned}\frac{\bar{E}_{\rm SA}(c,\delta)}{E_0} &= \frac{2\arcsin(c)}{c\sqrt{1-c^2}+\arcsin(c)} \\ &\times\left(\frac{2[2+\delta(2+\delta)]}{3(1+\delta)^2}-\frac{\mathcal{K}\left[\frac{\delta(2+\delta)}{(1+\delta)^2}\right]}{3(1+\delta)^2\mathcal{E}\left[\frac{\delta(2+\delta)}{(1+\delta)^2}\right]}\right) \\ &= \frac{2\arcsin(c)}{c\sqrt{1-c^2}+\arcsin(c)}\bar{E}(\omega=0,\delta), \end{aligned} \tag{36}$$

where $1 \geqslant c = \frac{tL}{A} = \frac{tL}{2\pi}\frac{\sqrt{\delta(2+\delta)}}{\sqrt{\delta(2+\delta)}+(1+\delta)^2\,\mathrm{s}^{-1}(1+\delta)}$ is the average surface density of the filament, t is the thickness of the filament, and A is the surface area of the ellipsoids. Nevertheless, when the flattening, δ, is large enough, it is clear that even a self-avoiding system will prefer to minimize the bending energy by avoiding the poles. Since any self-intersecting configuration must do this many times, proportionate to the filament density c, and by denoting the self-interaction energy per unit length in u, we can express the energy of a self-crossing filament as $\bar{E}+uc$ ($u>0$ for self-avoidance). Thus, the condition of a self-interacting filament to change from a polar configuration to a nonpolar one is

$$\bar{E}_{\rm SA}(c,\delta) \gtrsim \bar{E}(\omega_m(\delta)) + uc, \tag{37}$$

as this expression means that the energy of a nonintersecting, self-avoiding curve is larger than that of a self-interacting curve, including the self-interaction term. At small c's, $\bar{E}_{\rm SA}(c,\delta) \simeq \bar{E}(\omega=0,\delta)(1+\frac{c^2}{3})$. Expanding $\delta^* = \delta_0^* + \delta_1^* c$, where $\delta_0^* = 2.917$ is the critical δ found earlier, and requiring equality in Eq. (37), using Eq. (36) gives us the dependence of δ^* on c,

$$\bar{E}(0,\delta_0^*+c\delta_1^*)\left(1+\frac{c^2}{3}\right) = \bar{E}(\omega_m(\delta_0^*+c\delta_1^*))+uc. \tag{38}$$

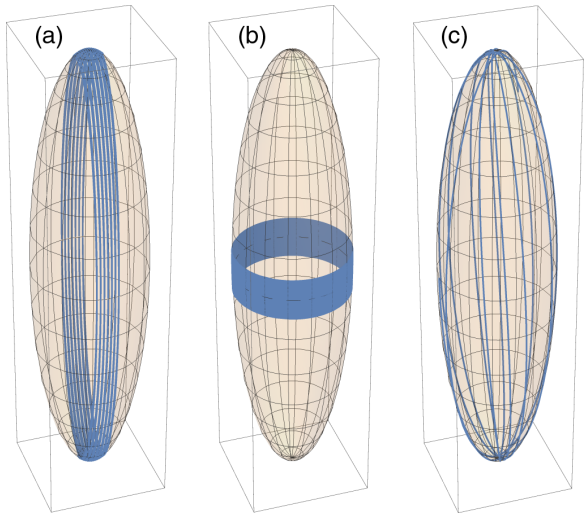

FIG. 5. Three examples emphasizing the effect of self-avoidance on prolate spheroid packing. (a) A self-avoiding polar geodesic-like state. (b) A self-avoiding equatorial geodesic-like state, which might be a metastable state. (c) A non-self-avoiding, geodesic solution with $\omega = 0.01$, self-crossing many times.

Expanding in orders of c and keeping only leading orders, the above equation reduces to

$$c\delta_1^*\left.\frac{\partial\bar{E}(0,\delta)}{\partial\delta}\right|_{\delta\to\delta_0^{*+}} = uc + c\delta_1^*\left.\frac{\partial\bar{E}(\omega_m(\delta))}{\partial\delta}\right|_{\delta\to\delta_0^{*+}}. \tag{39}$$

This can then be solved for δ_1^*,

$$\delta_1^* = \left.\frac{u}{\frac{\partial\bar{E}(0,\delta)}{\partial\delta}-\frac{\partial\bar{E}(\omega_m(\delta))}{\partial\delta}}\right|_{\delta\to\delta_0^{*+}}. \tag{40}$$

Since $\frac{\partial\bar{E}(0,\delta)}{\partial\delta}|_{\delta\to\delta_0^{*+}} \geqslant 0$ and $\frac{\partial\bar{E}(\omega_m(\delta))}{\partial\delta}|_{\delta\to\delta_0^{*+}} < 0$, it is clear that $\delta_1^* > 0$, therefore self-avoidance indeed postpones the aforementioned transition.

Another possible effect of self-avoidance is the appearance of metastable states, where the filament packs without crossing, such as paths with $\omega \sim 1$ that wrap many times around the ellipsoid [see Fig. 5(b)], but any deviation from this configuration means that the filament must cross itself many times [Fig. 5(c)]. At high densities and strong self-avoiding interactions, such a configuration is likely to be metastable.

IV. CONCLUSIONS AND DISCUSSION

To conclude, we have used a geometrical approach to show that the shape of an ellipsoid acts as an "external field" that orders the orientation of a stiff filament on its surface. We have shown that energy, not only entropy, plays a significant role in ordering the packing of filaments inside nonspherical volumes. With the use of geodesics to allow for a simple analytical treatment, we have directly shown that in general, filaments will tend to align with the long dimension of the ellipsoid. However, this is not completely accurate, since (at least for geodesics) the transition is likely to occur in very long ellipsoids, where the globally bending minimizing curve no

longer passes through the poles. The transition is somewhat sensitive to the geometry. For example, within a model of a cylinder with spherical caps, no such transition will occur as a function of elongation as the curvature does not depend on the the flattening in such a case. Nevertheless, these results reflect a similar numerical result to that in [9,40], specifically that the transition described in this paper echoes numerical results found in the context of microtubules [22,23,27,31], and the folded toroid to twisted toroid transition described by [28–30] in the context of viral capsids. Additionally, most wild-type viral capsids have a relatively small flattening, which is below the transition found here, namely $\delta < \delta^*$. The results shown here suggest that when a shape is too eccentric, the packing of genetic material will not be as efficient with respect to injection into a host cell. When applied to the ordering of MT along cell walls, these results suggest that ordering does not necessitate any biological means of actively or passively sensing stress within the cell wall. Hence, sensitivity to stress/strain by proxy, namely the integral over strain, leads to anisotropy. Finally, the treatment shown here is simplified, and it does not fully take into consideration any entropic effect and geometric effect such as self-avoidance. In any real system, temperature and/or activity plays a significant role, as does self-avoidance [2,3,41], and should be taken into account. Additionally, dynamics [23], friction effects [42] (both dynamic and static), plasticity of either the membrane or the filaments [42], and electrostatics [27] were not taken into account and are likely to play roles in different systems. In this context, the results shown here are an important stepping stone. A full statistical mechanical treatment that takes into account both entropy and self-avoidance is postponed for a later paper.

ACKNOWLEDGMENTS

The authors acknowledge the critical contribution of Enrico Coen, who pointed out the incomplete view on MT orientation in plant cells, and who motivated this work.

APPENDIX A: STABILITY ANALYSIS

For stability analysis we use a somewhat different and much more technical approach than the one presented in the main text. Most notably, we use an indexless notation, since an index notation will be much more cumbersome and definitely more complex to read. The analysis presented here is based on standard differential geometry, as can be found, for example, in [38]. We begin by rewriting our energy expression [Eq. (1)] for a general curve, parametrized generally [Eq. (A1)], that is not necessarily using the natural parametrization of arc-length $|R'(s)| = 1$. Soon after, we rigorously define a variation of the curve on a differential manifold, which allows us to define a variational field, which is the infinitesimal of a variation about the curve. This allows us to calculate the first and, more importantly, the second variations of our energy functional.

We begin by marking a general curve $c(s)$. The tangent to that curve is $\bar{\nabla}_s c = \frac{Dc}{Ds} = \frac{\partial c}{\partial s} = \dot{c}$. The energy we are seeking to minimize is then

$$\bar{E} = \frac{E}{L} = \frac{\int \left(\frac{\langle \bar{\nabla}_s \dot{c}, \bar{\nabla}_s \dot{c} \rangle}{\langle \dot{c}, \dot{c} \rangle^2} - \frac{\langle \bar{\nabla}_s \dot{c}, \dot{c} \rangle^2}{\langle \dot{c}, \dot{c} \rangle^3} \right) \sqrt{\langle \dot{c}, \dot{c} \rangle}\, ds}{\int \sqrt{\langle \dot{c}, \dot{c} \rangle}\, ds}$$
$$= \frac{\int \frac{\langle \bar{\nabla}_s \dot{c}, \bar{\nabla}_s \dot{c} \rangle}{\langle \dot{c}, \dot{c} \rangle^{3/2}}\, ds}{\int \sqrt{\langle \dot{c}, \dot{c} \rangle}\, ds}, \tag{A1}$$

where we omitted the second term in the first integral since it will prove to contribute exactly nothing in the following calculations. $\bar{\nabla}$ is the connection in the ambient space ($\mathbb{R}^3$), and $\langle X, Y \rangle$ is the inner product (metric) of two vectors X, Y. $\dot{c} \equiv \frac{\partial c}{\partial s} = \bar{\nabla}_s c$ since c is a scalar defined on the ellipsoid. Note that this form of writing is almost identical to Eq. (1), with the difference being that we may parametrize the curve in any way we want, therefore we include in the expression of $\langle \bar{\nabla}_s \dot{c}, \bar{\nabla}_s \dot{c} \rangle$ a tangent term $\langle \dot{c}, \bar{\nabla}_s \dot{c} \rangle$ and a normalization $\langle \dot{c}, \dot{c} \rangle$. Since eventually we will use arc-length parametrized curves (in fact, geodesics), this term will vanish.

A variation, $h(s,t)$, of a curve $c(s)$ is a two-parameter function $[s \in [0, L], t \in (-\epsilon, \epsilon)]$, such that $h(s,0) = c(s)$, and $h(0,t) = c(0)$, $h(L,t) = c(L)$. $h(s,t) \equiv c_t(s)$ for a given t is some curve meandering about $c(s)$. The field $v(s) = \frac{\partial h}{\partial t}(s,0)$ is called the variational field. Furthermore, close to $c(s)$, one can write $h(s,t)$ locally, without loss of generality, as $h(s,t) = \exp_{c(s)}(t v(s))$, where $\exp_p(v) \equiv \gamma(p,1,v)$ is the exponential map about a point p [a step of "length" 1 along a geodesic $\gamma(p,\lambda,v)$, so that $\gamma(p,0,v) = p$, $\dot{\gamma}(p,0,v) = \frac{\partial \gamma(p,\lambda,v)}{\partial \lambda}_{\lambda=0} = v$]. Finally, the nth variation of a functional $F[c(s)]$ is then found by $\delta^n F = \frac{1}{n!} \frac{d^n F[h(s,t)]}{dt^n}|_{t=0}$.

Thus

$$\bar{E}(t) = \frac{E(t)}{L(t)} = \frac{\int \frac{\langle \bar{\nabla}_s \dot{h}, \bar{\nabla}_s \dot{h} \rangle}{\langle \dot{h}, \dot{h} \rangle^{3/2}}\, ds}{\int \sqrt{\langle \dot{h}, \dot{h} \rangle}\, ds}, \tag{A2}$$

and we look for extrema by requiring a vanishing first variation $\delta \bar{E}$,

$$\delta \bar{E} = \frac{\delta E}{L} - \frac{E}{L}\frac{\delta L}{L} = \frac{\delta E}{L} - \bar{E}\frac{\delta L}{L} = 0, \tag{A3}$$

so that $\delta L = 0$ (i.e., curves are geodesics), and $\delta E = 0$ (they are extrema of the energy). In this case, it is easy to show that the second variation is then

$$\delta^2 \bar{E} = \frac{\delta^2 E}{L} - \bar{E}\frac{\delta^2 L}{L}. \tag{A4}$$

Since L is the length of a curve, its minimizers are geodesics:

$$2\delta L = 2\int \frac{d}{dt}\sqrt{\langle \dot{h}, \dot{h} \rangle}\, ds = \int \frac{\langle \bar{\nabla}_t \bar{\nabla}_s h, \bar{\nabla}_s h \rangle}{\sqrt{\langle \dot{h}, \dot{h} \rangle}}\, ds$$
$$\overset{t=0}{=} \int \frac{\langle \bar{\nabla}_s v, \dot{c} \rangle}{\sqrt{\langle \dot{c}, \dot{c} \rangle}}\, ds = \int \frac{d}{ds}\left(\frac{\langle v, \dot{c} \rangle}{\sqrt{\langle \dot{c}, \dot{c} \rangle}} \right) ds$$
$$- \int \frac{\langle v, \bar{\nabla}_s \dot{c} \rangle}{\sqrt{\langle \dot{c}, \dot{c} \rangle}} - \frac{\langle v, \dot{c} \rangle \langle \dot{c}, \bar{\nabla}_s \dot{c} \rangle}{\sqrt{\langle \dot{c}, \dot{c} \rangle}^3}\, ds. \tag{A5}$$

The first term is identically zero as it is a full derivative term and $v = 0$ at the boundary (even when they are taken to infinity). As for the second term, we note that it vanishes iff $c(s) = \gamma(s)$ is a geodesic. In that case, $\langle \dot\gamma, \bar\nabla_s \dot\gamma\rangle = 0$ is immediately satisfied (by the very definition of a geodesic), and $\bar\nabla_s \dot\gamma = \mathbf{B}(\dot\gamma, \dot\gamma)\hat n$, where $\mathbf{B}(X, Y) = \langle \bar\nabla_Y X, \hat n\rangle$ is the second fundamental form and $\hat n$ is the surface normal. Since $v \perp \hat n$ (it is a derivative of a scalar, hence it is tangent to the surface), we immediately get in such a case that $\langle v, \bar\nabla_s \dot\gamma\rangle = 0$.

Thus geodesics are extremal curves if

$$0 = \delta E = \int \delta\langle \bar\nabla_s \dot h, \bar\nabla_s \dot h\rangle - \frac{3}{2}\langle \bar\nabla_s \dot\gamma, \bar\nabla_s \dot\gamma\rangle \delta\langle \dot h, \dot h\rangle \, ds|_{t=0}$$
$$= \int \delta\langle \bar\nabla_s \dot h, \bar\nabla_s \dot h\rangle, \tag{A6}$$

where we used the fact that we are on geodesics, hence $\delta\langle \dot h, \dot h\rangle$ is zero, as has just been verified. It is readily seen that

$$\int \delta\langle \bar\nabla_s \dot h, \bar\nabla_s \dot h\rangle \, ds$$
$$= \int ds \frac{d}{dt}\langle \bar\nabla_s \dot h, \bar\nabla_s \dot h\rangle|_{t=0}$$
$$= 2\int ds \, \langle \bar\nabla_t \bar\nabla_s \dot h, \bar\nabla_s \dot h\rangle$$
$$= 2\int ds \left\langle \bar\nabla_s^2 v, \bar\nabla_s \dot\gamma\right\rangle$$
$$= 2\int ds \, \mathbf{B}(\dot\gamma, \dot\gamma)\left\langle \bar\nabla_s^2 v, \hat n\right\rangle, \tag{A7}$$

where we used the fact that we are embedded in flat Euclidean space, hence covariant derivatives, $\bar\nabla$, commute as the Riemann tensor vanishes. Using the fact that one can decompose $\bar\nabla = \nabla + \nabla^\perp$, where ∇ ($\equiv \nabla^\top$) is the connection on the tangent bundle of our ellipsoid, and $\nabla^\perp$ is the normal connection,

$$\left\langle \bar\nabla_s^2 v, \hat n\right\rangle = \left\langle \bar\nabla_s\left(\nabla_s^\perp v + \nabla_s^\top v\right), \hat n\right\rangle$$
$$= \left\langle {\nabla_s^\top}^2 v + \nabla_s^\perp \nabla_s^\top v + \bar\nabla_s \nabla_s^\perp v, \hat n\right\rangle. \tag{A8}$$

The first term on the right-hand side vanishes, since by definition the connection on the tangent bundle vanishes on the normal bundle, $\langle \nabla_Y^\top X, \hat n\rangle = 0$, and $\frac{d}{ds}\mathbf{B}(X, Y) = \bar\nabla_s\langle \bar\nabla_Y X, \hat n\rangle = \langle \bar\nabla_s \bar\nabla_Y X, \hat n\rangle + \langle \bar\nabla_Y X, \bar\nabla_s \hat n\rangle$. Additionally, $\bar\nabla_X \hat n = \nabla_X^\top \hat n$ for any X by virtue of $\hat n$ being a unit vector. We thus get

$$\left\langle \bar\nabla_s^2 v, \hat n\right\rangle = \mathbf{B}\left(\nabla_s^\top v, \dot\gamma\right) + \frac{d}{ds}\mathbf{B}(v, \dot\gamma), \tag{A9}$$

and from the definition of the covariant derivative of $\mathbf{B}$, together with the definition of a geodesic curve $\nabla_s \dot\gamma = 0$,

$$\left\langle \bar\nabla_s^2 v, \hat n\right\rangle = \mathbf{B}(\nabla_s v, \dot\gamma) + \left(\nabla_s^\perp \mathbf{B}\right)(v, \dot\gamma)$$
$$+ \mathbf{B}(\nabla_s v, \dot\gamma) + \mathbf{B}(v, \nabla_s \dot\gamma) \tag{A10}$$

$$= (\bar\nabla_s \mathbf{B})(v, \dot\gamma) + 2\mathbf{B}(\nabla_s v, \dot\gamma). \tag{A11}$$

Thus, δE is zero iff either γ is an asymptotic curve [in which case $\mathbf{B}(\dot\gamma, \dot\gamma)$ is zero], or if γ is locally a principal curve that is tangent to the principal directions of $\mathbf{B}$. The latter can be seen by noting that around a geodesic, we may restrict ourselves to variational fields v that are perpendicular to the curve without any loss of generality, as any tangent component of v translates into reparametrization of the geodesic. As a result, if γ is also a principal curve, then v always points in the other principal direction, and so does $\nabla_s v$, as can be seen directly by taking the derivative along the geodesic of $\langle v, \dot\gamma\rangle = 0$. Therefore, $\mathbf{B}(v, \dot\gamma)$ and $\mathbf{B}(\bar\nabla_s v, \dot\gamma)$ are identically zero.

To summarize, geodesics that are either asymptotic curves or principal curves are extrema of $\bar E$. To analyze their stability, we need to calculate the second variation. It is easily shown that around a geodesic curve,

$$L\delta^2 \bar E$$
$$= \int ds\left[\delta^2\langle \bar\nabla_s \dot h, \bar\nabla_s \dot h\rangle - \frac{1}{2}(3\langle \bar\nabla_s \dot\gamma, \bar\nabla_s \dot\gamma\rangle + \bar E)\delta^2\langle \dot h, \dot h\rangle\right]. \tag{A12}$$

Note that around our extrema,

$$\delta^2\langle \bar\nabla_s \dot h, \bar\nabla_s \dot h\rangle = \frac{1}{2}\frac{d^2}{dt^2}\langle \bar\nabla_s \dot h, \bar\nabla_s \dot h\rangle. \tag{A13}$$

Hence

$$2L\delta^2 \bar E$$
$$= \int ds\left[\frac{d^2}{dt^2}\langle \bar\nabla_s \dot h, \bar\nabla_s \dot h\rangle - \frac{1}{2}[3\mathbf{B}(\dot\gamma, \dot\gamma)^2 + \bar E]\frac{d^2}{dt^2}\langle \dot h, \dot h\rangle\right]. \tag{A14}$$

Now [38],

$$\frac{1}{2}\frac{d^2}{dt^2}\langle \dot h, \dot h\rangle = \langle \nabla_s v, \nabla_s v\rangle - K\langle v, v\rangle, \tag{A15}$$

where K is the Gaussian curvature.

Therefore,

$$\frac{1}{2}\frac{d^2}{dt^2}\langle \bar\nabla_s \dot h, \bar\nabla_s \dot h\rangle = \frac{d}{dt}\left\langle \bar\nabla_s^2 \partial_t h, \bar\nabla_s \dot h\right\rangle$$
$$= \left\langle \bar\nabla_s^2 \bar\nabla_t \partial_t h, \bar\nabla_s \dot h\right\rangle + \left\langle \bar\nabla_s^2 v, \bar\nabla_s^2 v\right\rangle. \tag{A16}$$

Calculating it term by term (starting with the first), using the fact that v is a tangent to a geodesic along t, and hence $\bar\nabla_t v$ is in the normal bundle,

$$\left\langle \bar\nabla_s^2 \bar\nabla_t \partial_t h, \bar\nabla_s \dot h\right\rangle = \left\langle \bar\nabla_s^2(\mathbf{B}(v, v)\hat n), \mathbf{B}(\dot\gamma, \dot\gamma)\hat n\right\rangle$$
$$= \mathbf{B}(\dot\gamma, \dot\gamma)\left\langle \nabla_s^\perp \bar\nabla_s(\mathbf{B}(v, v)\hat n), \hat n\right\rangle. \tag{A17}$$

A direct expansion yields

$$\bar\nabla_s(\mathbf{B}(v, v)\hat n) = \frac{d}{ds}\mathbf{B}(v, v)\hat n + \mathbf{B}(v, v)(-S_{\hat n}\dot\gamma)$$
$$= (\bar\nabla_s \mathbf{B})(v, v)\hat n + 2\mathbf{B}\left(\nabla_s^\top v, v\right)\hat n - \mathbf{B}(v, v)S_{\hat n}\dot\gamma, \tag{A18}$$

where $S_{\hat n}x = -\nabla_x \hat n = -\sum_{i=1,2}\langle \nabla_x \hat n, e_i\rangle e_i$ is the shape operator along x (e_i are an orthonormal frame on the surface). It is immediately apparent that

$$\nabla_s^\perp \bar\nabla_s(\mathbf{B}(v, v)\hat n) = \frac{d}{ds}(\bar\nabla_s \mathbf{B})(v, v)\hat n + 2\frac{d}{ds}\mathbf{B}\left(\nabla_s^\top v, v\right)\hat n$$
$$- \mathbf{B}(v, v)\nabla_s^\perp(S_{\hat n}\dot\gamma). \tag{A19}$$

From the shape operator definition, it is clear that

$$\nabla_s^{\perp}(S_{\hat{n}}\dot{\gamma}) = -\nabla_s^{\perp}\sum_i \langle \nabla_s \hat{n}, e_i\rangle e_i = \nabla_s^{\perp}\sum_i \mathbf{B}(\dot{\gamma}, e_i)e_i = \sum_i \mathbf{B}^2(\dot{\gamma}, e_i)\hat{n}. \tag{A20}$$

We thus conclude that

$$\begin{aligned}\left\langle \bar{\nabla}_s^2\bar{\nabla}_t\partial_t h, \bar{\nabla}_s\dot{h}\right\rangle\big|_{t=0} &= \mathbf{B}(\dot{\gamma},\dot{\gamma})\left[\frac{d}{ds}(\bar{\nabla}_s\mathbf{B})(v,v) + 2\frac{d}{ds}\mathbf{B}\left(\nabla_s^{\top}v, v\right) - \sum_i \mathbf{B}(v,v)\mathbf{B}^2(\dot{\gamma}, e_i)\right] \\ &= \mathbf{B}(\dot{\gamma},\dot{\gamma})\left[\frac{d}{ds}(\bar{\nabla}_s\mathbf{B})(v,v) + 2\frac{d}{ds}\mathbf{B}\left(\nabla_s^{\top}v, v\right)\right] - K\,\mathbf{B}^2(\dot{\gamma},\dot{\gamma})\langle v, v\rangle,\end{aligned} \tag{A21}$$

where we used the fact that γ is a geodesic, which is also a principal curve, and that $\langle v, \dot{\gamma}\rangle = 0$. Thus $\mathbf{B}(\dot{\gamma}, e_i) = k_\gamma\sqrt{\langle\dot{\gamma},\dot{\gamma}\rangle}$ if e_i points along $\dot{\gamma}$, and 0 otherwise. k_γ is the principal curvature along γ. Similarly, $\mathbf{B}(v,v) = k_v\langle v, v\rangle = k_v\|v\|^2$. Finally, $K = k_\gamma k_v$.

We thus conclude that

$$\begin{aligned}L\delta^2\bar{E} &= \int ds\left\{\left(\left\|\bar{\nabla}_s^2 v\right\|^2 + \mathbf{B}(\dot{\gamma},\dot{\gamma})\left[\frac{d}{ds}(\bar{\nabla}_s\mathbf{B})(v,v) + 2\frac{d}{ds}\mathbf{B}\left(\nabla_s^{\top}v, v\right)\right] - K\,\mathbf{B}^2(\dot{\gamma},\dot{\gamma})\|v\|^2\right)\right. \\ &\quad \left. -\frac{1}{2}[3\mathbf{B}^2(\dot{\gamma},\dot{\gamma}) + \bar{E}](\|\nabla_s v\|^2 - K\|v\|^2)\right\} \\ &= \int ds\left\{\left\|\bar{\nabla}_s^2 v\right\|^2 - \frac{1}{2}[3\mathbf{B}^2(\dot{\gamma},\dot{\gamma}) + \bar{E}]\|\bar{\nabla}_s v\|^2 + \frac{K}{2}[\mathbf{B}^2(\dot{\gamma},\dot{\gamma}) + \bar{E}]\|v\|^2 + \mathbf{B}(\dot{\gamma},\dot{\gamma})\frac{d^2}{ds^2}\mathbf{B}(v,v)\right\}.\end{aligned} \tag{A22}$$

Integrating by parts the last expression twice yields

$$L\delta^2\bar{E} = \int ds\left\{\left\|\bar{\nabla}_s^2 v\right\|^2 - \frac{1}{2}[3\mathbf{B}^2(\dot{\gamma},\dot{\gamma}) + \bar{E}]\|\bar{\nabla}_s v\|^2 + \frac{K}{2}[\mathbf{B}^2(\dot{\gamma},\dot{\gamma}) + \bar{E}]\|v\|^2 + \mathbf{B}(v,v)\frac{d^2}{ds^2}\mathbf{B}(\dot{\gamma},\dot{\gamma})\right\}. \tag{A23}$$

It is immediately seen that on a sphere [by setting $K = 1$, $\mathbf{B}(X, Y) = 1$]

$$L\delta^2\bar{E}_{\text{sphere}} = \int ds\left(\left\|\bar{\nabla}_s^2 v\right\|^2 - 2\|\bar{\nabla}_s v\|^2 + \|v\|^2\right). \tag{A24}$$

Using Fourier analysis, it is easily shown that this expression is stable with respect to all variational fields v except $v = v_0\exp(is)$, where it vanishes. This means that every variation around a geodesic (which is, by default, a principal direction) is stable (i.e., geodesics are stable solutions) except ones that oscillate with a periodicity of the sphere's circumference. Such a variation is merely another (nearby) great circle (and only great circles are geodesics on a sphere).

By expressing $\mathbf{B}(X, Y)$ for polar geodesics ($\omega = 0$), and expanding the expressions in small $\delta > 0$, it can be shown that instability occurs for wave numbers (around polar geodesics)

$$1 - \sqrt{2\delta} < \lambda < 1 + \sqrt{2\delta}, \tag{A25}$$

hence polar geodesics are unstable for all $\delta > 0$. For $\delta < 0$ all, equatorial geodesics are always stable since

$$\begin{aligned}&L\delta^2\bar{E}(\delta < 0) \\ &\quad \simeq \int ds\left(\left\|\bar{\nabla}_s^2 v\right\|^2 - 2\|\bar{\nabla}_s v\|^2 + \|v\|^2 + 2|\delta|\|v\|^2\right) > 0.\end{aligned} \tag{A26}$$

APPENDIX B: ESTIMATION OF STABLE SOLUTIONS

While one can produce better estimates, here we will use only a rough estimation to show that for $0 < \delta \ll 1$, κ_g must be small, too. The logic behind this argument is as follows: it is clear that a curve on the equator will, at least locally, prefer to point along the polar direction as the curvature is lowest along this direction. However, near the poles the curvature is larger even than that of the equatorial geodesic. It may therefore be preferential for the curve to change direction so that it bypasses the pole, even if only slightly. To bound the average geodesic curvature, we consider two cases: as an upper bound we consider a geodesic on a sphere having the same curvature as that at the pole ($l_{\max} = 1 + \delta$). Clearly, any physical solution on the ellipsoid has lower energy than that, since even a polar geodesic has lower energy. As for a lower bound, we now consider some configuration (with nonzero geodesic curvature) on a sphere whose curvature is equal to the lowest curvature on the ellipsoid ($l_{\min} = \frac{1}{(1+\delta)^2}$). In other words,

$$\begin{aligned}\bar{E}_{\text{lower}} &= \left\langle\kappa_g^2\right\rangle + l_{\min}^2 < \bar{E}_{\text{actual}} \\ &= \left\langle\kappa_g^2\right\rangle + \langle l^2(\kappa_g)\rangle < \bar{E}_{\text{higher}} = l_{\max}^2 \\ &\Rightarrow \left\langle\kappa_g^2\right\rangle < l_{\max}^2 - l_{\min}^2 = (1+\delta)^2 - 1/(1+\delta)^4 \\ &\overset{\delta\ll 1}{\simeq} 6\delta + O(\delta^2) \ll 1.\end{aligned} \tag{B1}$$

This is an extremely rough estimate, but it suffices in order to support our claim that for small δ the actual minimizing curve is almost a geodesic (and specifically a polar geodesic). Note that a localized highly curved region is not a possible solution since for any finite deviation from a geodesic assuming a localized curvature along some scale Δ, one must have $\kappa_g \propto 1/\Delta$. Furthermore, from the symmetry of the

problem, such regions must occur infinitely many times along the curve (if it occurs only a finite number of times, then we must sit on a geodesic). Hence the contribution to the mean energy $\Delta\bar{E} \propto (1/\Delta^2)\Delta = 1/\Delta \xrightarrow{\Delta\to 0} \infty$. Hence the globally minimizing curve must have a fairly uniform distribution of geodesic curvature along it (i.e., $\kappa_g \sim \text{const} \sim 2\sqrt{\delta} \ll 1$).

In the case of $\delta \gg 1$, a different argument takes over—in this limit, the polar direction has mostly zero curvature, except at a region near the poles where it is very large. Furthermore, the azimuthal curvature in these regions is also very high. Near the caps, deviation from the polar direction is therefore also very costly (as it is much larger than 1, the azimuthal curvature around the equatorial). Thus, a rod will prefer to avoid regions with high mean curvature (as it is affected by both the polar and azimuthal curvatures). A reasonable criterion is that the curve will remain (up to some penetration depth) in regions satisfying $\|\frac{1}{2}\mathrm{Tr}(S)\| \leqslant 1$. By finding the angle θ_1 at which it is equal to 1,

$$1 = \left\|\frac{1}{2}\mathrm{Tr}(S)\right\| = \frac{(1+\delta)[2+\delta(2+\delta)\sin^2\theta_1]}{2[1+\delta(2+\delta)\sin^2\theta_1]^{3/2}} \xrightarrow{\delta\gg 1} \frac{1}{2\sin\theta_1}, \tag{B2}$$

we see that the curve is limited to a region such that $\theta_1 \leqslant \theta(s) \leqslant \pi - \theta_1$, primarily pointing along the ellipsoid. Finally, direct calculation shows that $\theta_1 \geqslant 30^\circ$ (monotonically approaching 30° in the limit of $\delta \gg 1$). Hence, while in this case κ_g is not necessarily small (though it does not need to be too large either), the curve probes much of the surface of the ellipsoid as it traverses about 2/3 of its length.

APPENDIX C: SELF-AVOIDANCE

The energy of a close-packed, almost polar geodesic, path on the ellipsoid is approximated as the energy of $N = 2K + 1$ closed paths, so that each path is numbered by $|n| \leqslant K$, where $n = 0$ is the path passing through the poles, and other paths reside in a plane parallel to it. If the filament's thickness is given by t, it is not hard to see that the distance of each such filament from the plane bisecting the ellipsoid through the poles is given by $d = nt$. The relative distance y is the fraction $\frac{d}{D}$, where D is the semiminor axis length. For an ordered configuration of maximal width $d_{\max}$ we can show that up to a small correction, $y_{\max} \simeq c$, where $c = \frac{L_{\mathrm{tot}}t}{A}$ is the packing density, and L_{tot} is the total length of a filament. As each configuration is planar, it can be written as

$$\mathbf{f}(\varphi) = D(0, \sqrt{1-y^2}\sin\varphi, \sqrt{1-y^2}(1+\delta)\cos\varphi). \tag{C1}$$

A length element is given by

$$ds^2 = D^2(1-y^2)[\cos^2(\varphi) + (1+\delta)^2\sin^2(\varphi)]\,d\varphi^2, \tag{C2}$$

and the local curvature of the curve is given by

$$\kappa = \frac{1+\delta}{D\sqrt{1-y^2}[\cos^2(\varphi) + (1+\delta)^2\sin^2(\varphi)]^{3/2}}. \tag{C3}$$

Thus the total energy of a single path at y is

$$E(y) = \frac{1}{\sqrt{1-y^2}}E(\omega = 0), \tag{C4}$$

where $E(\omega = 0)$ is the energy of a polar path. The length of a single path is

$$L(y) = \sqrt{1-y^2}L(0) \tag{C5}$$

[$L(0)$ being the length of a polar path], so that

$$\bar{E}_{\mathrm{SA}} = \frac{\int E(y)\,dy}{\int L(y)\,dy} \simeq \frac{2\arcsin(c)}{4\pi c\sqrt{1-c^2} + \arcsin(c)}\bar{E}(\omega = 0). \tag{C6}$$

[1] D. Marenduzzo, C. Micheletti, and E. Orlandini, J. Phys.: Condens. Matter **22**, 283102 (2010).
[2] E. Katzav, M. Adda-Bedia, and A. Boudaoud, Proc. Natl. Acad. Sci. (USA) **103**, 18900 (2006).
[3] L. Boué and E. Katzav, Europhys. Lett. **80**, 54002 (2007).
[4] P. K. Purohit, J. Kondev, and R. Phillips, Proc. Natl. Acad. Sci. (USA) **100**, 3173 (2003).
[5] D. G. Angelescu and P. Linse, Soft Matter **4**, 1981 (2008).
[6] M. Uyttewaal, A. Burian, K. Alim, B. Landrein, D. Borowska-Wykrrt, A. Dedieu, A. Peaucelle, M. Ludynia, J. Traas, A. Boudaoud *et al.*, Cell **149**, 439 (2012).
[7] D. H. Burk and Z.-H. Ye, The Plant Cell **14**, 2145 (2002).
[8] N. B. Stoop, Ph.D. thesis, ETH Zurich (2011).
[9] R. Vetter, F. Wittel, N. Stoop, and H. Herrmann, Eur. J. Mech.-A **37**, 160 (2013).
[10] R. Vetter, Ph.D. thesis, ETH Zurich (2015).
[11] M. Pineirua, M. Adda-Bedia, and S. Moulinet, Europhys. Lett. **104**, 14005 (2013).
[12] H. Elettro, Ph.D. thesis, Institut D'Alembert, Équipe Mécanique et Ingénierie des Solides et des Structures, 2015.
[13] H. Elettro, F. Vollrath, A. Antkowiak, and S. Neukirch, Soft Matter **13**, 5509 (2017).
[14] H. Elettro, P. Grandgeorge, and S. Neukirch, J. Elast. **127**, 235 (2017).
[15] J. Elsner, M. Michalski, and D. Kwiatkowska, Ann. Botany **109**, 897 (2012).
[16] D. D. Fisher and R. J. Cyr, Plant Physiol. **116**, 1043 (1998).
[17] C. Somerville, S. Bauer, G. Brininstool, M. Facette, T. Hamann, J. Milne, E. Osborne, A. Paredez, S. Persson, T. Raab *et al.*, Science **306**, 2206 (2004).
[18] M. Sahaf and E. Sharon, J. Exp. Botany **67**, 5509 (2016).
[19] E. Oh, J.-Y. Zhu, M.-Y. Bai, R. A. Arenhart, Y. Sun, and Z.-Y. Wang, elife **3**, e03031 (2014).
[20] J. Chaiwanon, W. Wang, J.-Y. Zhu, E. Oh, and Z.-Y. Wang, Cell **164**, 1257 (2016).
[21] S. N. Fejer, in *Progress in Molecular Biology and Translational Science* (Elsevier, Amsterdam, 2020), Vol. 170, pp. 405–434.
[22] D. Marenduzzo, Europhys. Lett. **85**, 38005 (2009).
[23] I. Ali, D. Marenduzzo, and J. M. Yeomans, Phys. Rev. Lett. **96**, 208102 (2006).

[24] H. Wang, Z. Guo, H. Feng, Y. Chen, X. Chen, Z. Li, W. Hernández-Ascencio, X. Dai, Z. Zhang, X. Zheng *et al.*, J. Virology **92**, e01727-17 (2018).
[25] V. Krishna, G. S. Ayton, and G. A. Voth, Biophys. J. **98**, 18 (2010).
[26] V. B. Rao and G. Leffers, Virology **196**, 896 (1993).
[27] D. Marenduzzo, Comput. Math. Methods Med. **9**, 317 (2008).
[28] A. S. Petrov, M. B. Boz, and S. C. Harvey, J. Struct. Biol. **160**, 241 (2007).
[29] A. S. Petrov and S. C. Harvey, Biophys. J. **95**, 497 (2008).
[30] A. S. Petrov, C. R. Locker, and S. C. Harvey, Phys. Rev. E **80**, 021914 (2009).
[31] S. Jun and B. Mulder, Proc. Natl. Acad. Sci. (USA) **103**, 12388 (2006).
[32] I. Newton, *Philosophiae Naturalis Principia Mathematica* (Apud Guil. & Joh. Innys, Regiæ Societatis Typographos, 1726), Vol. 3.
[33] F. Bessel, Astron. Nachr. **4**, 241 (1825).
[34] F. Bessel, C. F. Karney, and R. E. Deakin, Astron. Nachr. **331**, 852 (2010).
[35] S. Panyukov and Y. Rabin, Phys. Rev. Lett. **85**, 2404 (2000).
[36] D. Grossman, E. Sharon, and H. Diamant, Phys. Rev. Lett. **116**, 258105 (2016).
[37] D. Grossman, E. Sharon, and E. Katzav, Phys. Rev. E **98**, 022502 (2018).
[38] M. P. Do Carmo, *Differential Geometry of Curves and Surfaces: Revised and Updated*, 2nd ed. (Courier Dover, Mineola, New York, 2016).
[39] F. W. Olver, D. W. Lozier, R. F. Boisvert, and C. W. Clark, *NIST Handbook of Mathematical Functions Hardback and CD-ROM* (Cambridge University Press, Cambridge, 2010).
[40] V. Mirabet, P. Krupinski, O. Hamant, E. M. Meyerowitz, H. Jönsson, and A. Boudaoud, PLoS Comput. Biol. **14**, e1006011 (2018).
[41] S. F. Edwards, Proc. Phys. Soc. **85**, 613 (1965).
[42] R. Vetter, F. K. Wittel, and H. J. Herrmann, Nat. Commun. **5**, 1 (2014).